Journal of Sound and Vibration (1984) **93**(3), 353–364

COMPUTER SIMULATION OF A SHOCK-ABSORBING PNEUMATIC CYLINDER

Y. T. WANG, R. SINGH, H. C. YU AND D. A. GUENTHER

Department of Mechanical Engineering, The Ohio State University, Columbus, Ohio 43210, *U.S.A.*

(*Received* 27 *September* 1982, *and in revised form* 18 *April* 1983)

A mathematical simulation model of a double-acting pneumatic cushioning cylinder, designed to absorb periodic shock loads, is presented, which is based on the following assumptions: ideal equation of state, isentropic flow through a port–bleed orifice, isentropic compression process, single degree of freedom piston–cylinder dynamics, and the energy-equivalent linear damping. Because of the non-linear differential equation and a requirement for simultaneous iterative solution, a computer simulation model is employed to predict pressure and motion time histories, and cylinder performance indices. Predictions for both untuned and tuned cylinder example cases are compared with measurements. Good correlations between simulation and experiment are evident even though empirical models for discharge coefficients and damping have been used. The computer simulation has been successful in evaluating a number of products, and thus can be used as a design tool. However, more experimental work must be done to improve its prediction capabilities.

1. INTRODUCTION

Pneumatic isolators and dampers are commonly employed for vibration and shock control. However, the published literature [1–9] available on such pneumatic components is limited, as documented by Hundal [6]. Pneumatic systems such as cylinders have received even less attention [10, 11]. Adams *et al.* [10] have shown that a computer simulation model is required to study a pneumatic cylinder because of the non-linear equations of motion; this study was a demonstrative modeling exercise as a constant forcing function was assumed for determining response. Wang *et al.* [11] have developed a simple mathematical model of a pneumatic cylinder subjected to an impulse or initial velocity excitation. This study has shown that the dimensionless formulations, as established for design purposes [1], are not adequate as these are based on the assumption of critical mass flow rate through the bleed orifice; in fact, a zero mass flow rate assumption is more suitable.

In this paper, a mathematical simulation model of a pneumatic cushioning cylinder subjected to high velocity cyclic shocks is presented. In contrast to previous studies [10, 11], all cylinder processes are considered to occur under realistic forcing functions as all instantaneous operating variables are updated continuously. The simulation model is validated by comparing results with those of an analogous experiment.

2. MATHEMATICAL FORMULATION

Figure 1 shows schematically a double-acting cushioning-type pneumatic cylinder with an attached load M_l. The inlet and outlet ends of the cylinder are assumed to be connected to two on–off type flow reservoirs; these reservoirs are considered to be out of phase with each other. The supply pressure p_s and temperature T_s are assumed to be constant. For analysis purposes, the gas space inside the cylinder is divided into four control volumes,

0022–460X/84/070353+12 $03.00/0

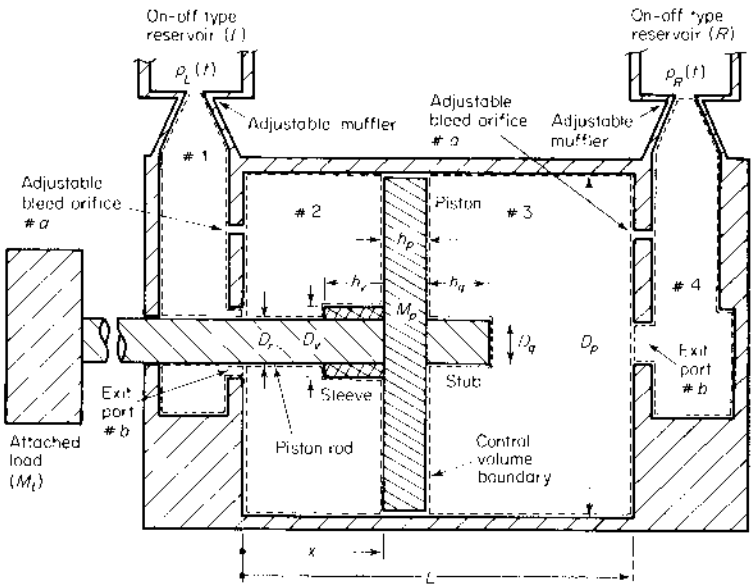

Figure 1. Schematic of a double-acting pneumatic cylinder.

as shown in Figure 1. It is assumed that no energy in the form of work or heat crosses the boundaries of the overall control volume enclosing the four control volumes. It is also assumed that the ideal equation of state with constant thermodynamic properties applies to the air (a list of symbols is given in the Appendix):

$$p_j(t)\,V_j(t) = Rm_j(t)\,T_j(t), \qquad j = 1, 2, 3, 4. \tag{1}$$

2.1. FLUID FLOW MODEL

Instantaneous mass flow rate ($\dot{m}$) through a port, orifice, or past piston rings can be described by the quasi-steady state isentropic flow process for an orifice [12, 13]:

$$\dot{m}_{ud}(t) = C_{ud}A_{ud}U_{ud}(x)p_u(t)\left[\frac{2\gamma g_c}{(\gamma-1)RT_u(t)}\right]^{1/2}\left[\left(\frac{p_d}{p_u}\right)^{2/\gamma} - \left(\frac{p_d}{p_u}\right)^{(\gamma+1)/\gamma}\right]^{1/2}. \tag{2}$$

The maximum mass flow rate is given by the critical pressure ratio $(p_d/p_u)_{\text{critical}} = [2/(\gamma+1)]^{\gamma/(\gamma-1)}$. Different mass flow rates along with appropriate upstream and downstream conditions are given in Table 1. Note that A_{23} is the leakage area, C_{23} is the discharge coefficient, and $\dot{m}_{23}$ is the leakage past the piston rings [14, 15].

2.2. PROCESS MODEL

The process is assumed to be isentropic, and pressure and temperature are assumed to be uniform within a control volume:

$$p_j(t)[V_j(t)/m_j(t)]^{\gamma} = p_j(0)[V_j(0)/m_j(0)]^{\gamma}, \qquad j = 1, 2, 3, 4. \tag{3}$$

The instantaneous mass of any control volume is

$$m_j(t) = m_j(0) + \int [\dot{m}_{ji}(t) - \dot{m}_{je}(t)]\,\mathrm{d}t, \qquad j = 1, 2, 3, 4. \tag{4}$$

Instantaneous mass and mass rates of different control volumes are given in Table 2. Initial conditions for mass flow rates are $\dot{m}_{ji}(0) = 0$, and $\dot{m}_{je}(0) = 0$.

TABLE 1

Mass flow rate table for equation (2)

$\dot{m}_{ud}$	u	d	A_{ud}	$U_{ud}(x)$	$p_u(t)$	$p_d(t)$
$\dot{m}_{L1}$	L	1	A_{L1}	$U(0)$	p_L	p_1
$\dot{m}_{12_a}$	1	2	A_{12_a}	$U(0)$	p_1	p_2
$\dot{m}_{12_b}$	1	2	A_{12_b}	$U(h_v)$	p_1	p_2
$\dot{m}_{23}$†	2	3	A_{23}†	$U(0)$	p_2	p_3
$\dot{m}_{34_a}$	3	4	A_{34_a}	$U(0)$	p_3	p_4
$\dot{m}_{34_b}$	3	4	A_{34_b}	$U(0)-U(S-h_q)$	p_3	p_4
$\dot{m}_{4R}$	4	R	A_{4R}	$U(0)$	p_4	p_R

† Leakage only.

TABLE 2

Instantaneous mass and mass flow rate table for equation (4)

m_j	$\dot{m}_{ji}$	$\dot{m}_{je}$
m_1	$\dot{m}_{L1}$	$\dot{m}_{12_a}+\dot{m}_{12_b}$
m_2	$\dot{m}_{12_a}+\dot{m}_{12_b}$	$\dot{m}_{23}$†
m_3	$\dot{m}_{23}$†	$\dot{m}_{34_a}+\dot{m}_{34_b}$
m_4	$\dot{m}_{34_a}+\dot{m}_{34_b}$	$\dot{m}_{4R}$

† Leakage only.

2.3. PISTON MOTION MODEL

A single degree of freedom lumped parameter model is assumed to describe the piston dynamics. With piston, piston rod and attached load treated as a rigid body, the total mass is $M_T = M_p + M_r + M_l$.

At any instant t, the pneumatic stiffness $K_f(t)$ of the chamber number 2 (or 3) is given by assuming the following: (i) isentropic compression process, (ii) no air escape from the volume at time t, (iii) linear system with small piston displacement, and (iv) perfectly elastic medium [16]:

$$K_{fj}(t) = \gamma p_j(t) A_j^2 / V_j(t), \qquad j = 2, 3. \tag{5}$$

This formulation has already been used successfully [11]. Here, operating variables p_j and V_j are computed iteratively by using the overall mathematical model. An energy-equivalent linear damping coefficient $B_T(t)$ is assumed to be applicable, which consists of both mechanical and fluid dampings. The total damping ratio ζ_T is defined as

$$\zeta_T = \zeta_m + \zeta_F = [B_m(t) + B_f(t)]/2(M_T K_T(t))^{1/2} = B_T(t)/2(M_T K_T(t))^{1/2}, \tag{6}$$

where K_T is the total stiffness, equal to $K_m + K_{fj}$. Here K_m is the mechanical stiffness, which is considered only during the mechanical impact, at $x = 0$ or S.

The equation of motion for the piston–cylinder arrangement is

$$M_T \ddot{x}(t) + 2\zeta(M_T K_T(t))^{1/2} \dot{x}(t) + K_m(t) x(t) = F(t), \qquad 0 \leqslant x \leqslant S. \tag{7}$$

The initial conditions are $\dot{x}(0) = 0$, and $x(0) = 0$ or S (depending on the operating conditions—see equations (12) and (13)). The forcing function $F(t)$ is due to the pressure differential across the piston and is given by the following general expression for the

double-acting case:

$$F(t) = p_1(t)(A_v - A_r)[U(0) - U(h_v)] + p_2(t)[(A_p - A_v)U(0) + (A_v - A_r)U(h_v)] - p_3(t)[A_pU(0) - A_qU(S - h_q)] - p_4(t)A_qU(S - h_q), \quad (8)$$

$$A_p = (\pi/4)D_p^2, \quad A_r = (\pi/4)D_r^2, \quad A_q = (\pi/4)D_q^2, \quad A_v = (\pi/4)D_v^2, \quad (9)$$

$$V_2(t) = (A_p - A_v)x(t) + (A_v - A_r)(x(t) - h_v)U(h_v), \quad V_3(t) = A_pS - V_2(t) - A_sh_q. \quad (10, 11)$$

It should be noted that the operating pressure terms are on both sides of equation (7) indicating pneumatic stiffness, damping and system input.

Ignoring the dynamics of the directional control valve, one can describe $p_R(t)$ and $p_L(t)$ as follows:

$$p_R(t) = p_sU(t) - p_sU(t + (S/\bar{x})) = p_R(t + (2S/\bar{x})), \quad (12a)$$

$$p_R(0) = p_s, \quad x(0) = 0, \quad \text{and} \quad p_R(0) = p_0, \quad x(0) = S, \quad (12b)$$

$$p_L(t) = p_s - p_R(t) = p_L(t + (2S/\bar{x})), \quad (13a)$$

$$p_L(0) = p_0, \quad x(0) = 0 \quad \text{and} \quad p_L(0) = p_s, \quad x(0) = S, \quad (13b)$$

where $\overline{x(t)}$ is the time-averaged piston velocity, computed numerically. It could be computed over the whole stroke S or over the time period of interest.

3. EXPERIMENT

To validate the mathematical simulation model, an experimental study has been conducted [17]. Figure 2 shows schematically the experimental stand along with the measurement system. Two strain gauge type pressure transducers are installed to measure $p_2(t)$ and $p_3(t)$. Ideally, these should be mounted flushed with the cylinder wall; however, a very small cavity in front of the transducer does not pose any practical problem.

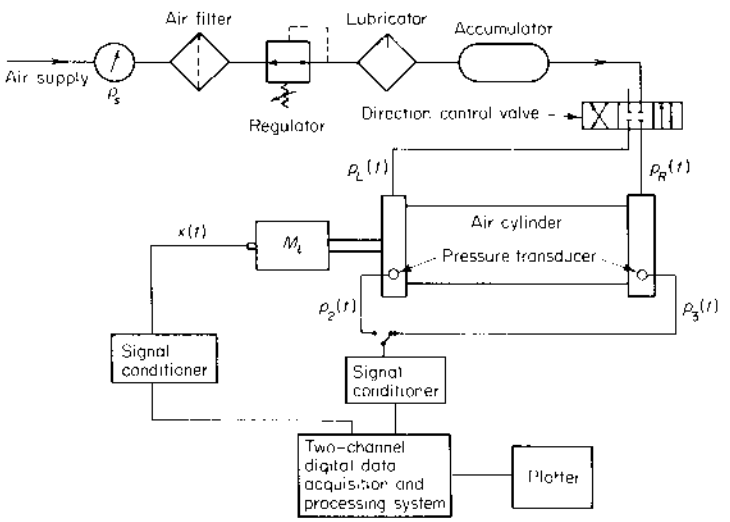

Figure 2. Schematic of the experiment and measurement system.

Nevertheless, such small cavity volumes are added to $V_2(0)$ and $V_3(0)$ in the computer simulation. A piezoelectric type accelerometer is placed on the attached load to measure $\ddot{x}(t)$.

4. EXAMPLE CASES

The air supply conditions, loads and geometrical values of the example cases used for experimentation and mathematical simulation are as follows:

(i) air supply conditions, $p_s = 0{\cdot}24$, $0{\cdot}38$, $0{\cdot}51$ and $0{\cdot}65$ MPa, $T_s = 293$–298°K; (ii) loads, $M_r + M_p = 1{\cdot}0$ kg, $M_l = 4{\cdot}5$, $6{\cdot}8$, $9{\cdot}1$ and $11{\cdot}4$ kg; (iii) geometry, $h_v = 46{\cdot}1$ mm, $h_q = 45{\cdot}2$ mm, $h_p = 31{\cdot}8$ mm, $D_v = 19{\cdot}0$ mm, $D_r = 15{\cdot}9$ mm, $D_q = 12{\cdot}6$ mm, $D_p = 63{\cdot}5$ mm, $S = 304{\cdot}8$ mm, $A_{12_b} = 84{\cdot}1$ mm^2, $A_{34_b} = 125{\cdot}2$ mm^2, $V_1 = 4095$ mm^3, $V_4 = 9830$ mm^3; (iv) adjustable bleed orifices and mufflers, as specified in Table 3.

TABLE 3

Adjustable bleed orifice and muffler throat areas

Example case	$A_{12_a} = A_{34_a}$ (mm^2)	$A_{1.1} = A_{4R}$ (mm^2)	M_l (kg)	p_s (MPa)	Remark
I Untuned cylinder	11·7	71·3	4·5	0·24, 0·38, 0·51, 0·65	Bleed orifices and muffler throats fully open
II Tuned cylinder	6·8	39·4	4·5	0·65	Bleed orifices and mufflers partially open; both tuned to ensure smooth operation
	6·8	35·5	6·8	0·65	
	6·8	34·2	9·1	0·65	
	6·8	33·6	11·4	0·65	

To achieve a smooth operation of the cylinder, the bleed orifice and muffler throat areas can be adjusted and tuned for a given load and velocity. Table 3 shows the following cases: (i) untuned cylinder—the adjustable bleed orifices and muffler throats are completely open; (ii) tuned cylinder—bleed orifices and muffler throats are partially open in order to obtain a smooth motion including stop. The tuned case, therefore, ensures small deceleration values and lower mechanical impacts and oscillations.

5. COMPUTER SIMULATION

A computer simulation program is rquired to solve for operating variables because (i) equation of motion (7) is non-linear and contains time-varying coefficients, and (ii) a simultaneous solution of equations (1)–(13) is needed. We have employed the IBM-CSMP III as the simulation language for our computations [18, 19]. For a desired simulation duration of $t = 0$–500 ms, a very small time increment ($0{\cdot}25$ ms) was used for efficient and accurate computations. The desired output contains pressure and motion time histories. From this data base the following performance indices often used for design evaluation [1, 11, 17] were determined: peak compression pressures in chambers p_2^* and p_3^*, peak deceleration $\ddot{x}^*$, time-averaged piston velocity $\overline{\dot{x}(t)}$, kinetic energy absorbed, etc.

5.1. SELECTION OF PARAMETERS

Knowledge of the following parameters is vital for the computer simulation model: A_{23}, C_{ad}, and ζ_T. Since it is difficult to assess these theoretically, empirical formulations

or experiment-based data are often utilized [1, 10]. For our simulation study, we assumed the following somewhat *arbitrarily*, based on our *intuition* and *experience*: (i) negligible leakage area, $A_{23}=0$; (ii) all discharge coefficients (C_{ud}) are equal to a constant value C such that C is not a function of the operating conditions; (iii) the damping ratio $\zeta_T=\zeta_T(p_s)$.

A number of simulation functions for ζ and C were selected in order to study their effects on the cylinder performance [19]. For the results given in this paper, the following values were chosen:

$$C=0{\cdot}65, \tag{14}$$

$$\zeta_T=\begin{cases} 0{\cdot}53p_s, & 0\leqslant p_s\leqslant 0{\cdot}38\ \text{MPa} \\ -0{\cdot}34+1{\cdot}42p_s, & 0{\cdot}38\leqslant p_s\leqslant 0{\cdot}59\ \text{MPa} \\ 0{\cdot}5, & p_s\geqslant 0{\cdot}59\ \text{MPa} \end{cases}. \tag{15}$$

Initial conditions for the computer simulation were as follows:

$$\begin{aligned} &\dot{m}_{ji}(0)=\dot{m}_{je}(0)=0, \qquad \dot{x}(0)=0, \\ &x(0)=0, \qquad p_R(0)=p_s \quad \text{and} \quad p_L(0)=p_0, \\ &x(0)=S, \qquad p_R(0)=p_0 \quad \text{and} \quad p_L(0)=p_s. \end{aligned} \tag{16}$$

6. RESULTS

Table 4 shows predicted results compared with measured data for an untuned cylinder. Excellent agreement between simulation and experiment is evident for $\ddot{x}^*$, but such agreement is not evident for p_3^* at low and high supply pressures; however, at the mid-supply pressure range, the correlation is excellent. In practice a pneumatic cylinder is always tuned to a given load, otherwise the cylinder cannot function as a shock-absorber.

TABLE 4

Comparison of results for the untuned cylinder: example case I

		p_3^*			$\ddot{x}^*$		
			Predicted			Predicted	
p_s (MPa)	M_l (kg)	Measured (MPa)	(MPa)	Error† (%)	Measured (g)	(g)	Error† (%)
0·24	4·5	1·6	1·4	12·5	69	66	4·3
0·38	4·5	2·6	2·5	3·8	131	131	0
0·51	4·5	3·3	3·2	3·0	162	165	−1·9
0·65	4·5	3·6	4·4	−22·2	229	221	3·6

† Error = 100 (Measured − Predicted)/Measured.

For an untuned cylinder, the piston does not come to a gradually smooth stop; rather it impacts against the port wall. For example, $\ddot{x}^*$ values in Table 4 are very high and indicate acceleration rather than deceleration. Although this example case presented here is only an *academic exercise*, the computer simulation is still able to predict the cylinder performance accurately.

Results for the practical case, i.e., a tuned cylinder, are presented in Table 5. Smaller $\ddot{x}^*$ values, as compared to example case I, are evident; these represent peak decelerations.

TABLE 5

Comparison of results for the tuned cylinder: example case II

M_l (kg)	p_s (MPa)	p_3^* Measured (MPa)	p_3^* Predicted (MPa)	p_3^* Predicted Error† (%)	$\ddot{x}^*$ Measured (g)	$\ddot{x}^*$ Predicted (g)	$\ddot{x}^*$ Predicted Error† (%)	Cushion Entrance Velocity Measured‡ (m/s)	Cushion Entrance Velocity Predicted (m/s)	Cushion Entrance Velocity Predicted Error† (%)
4·5	0·65	0·69	0·71	−2·9	12·8	13·2	−3·1	1·56	1·49	4·5
6·8	0·65	0·72	0·72	0	9·8	9·2	6·1	1·39	1·26	9·4
9·1	0·65	0·72	0·72	0	7·4	6·9	6·8	1·24	1·06	14·5
11·4	0·65	0·72	0·74	−2·8	6·5	6·0	8·3	1·19	1·01	15·1

† Error = 100 (Measured − Predicted)/Measured.

‡ Measured velocity is estimated using the piston acceleration time history data obtained experimentally.

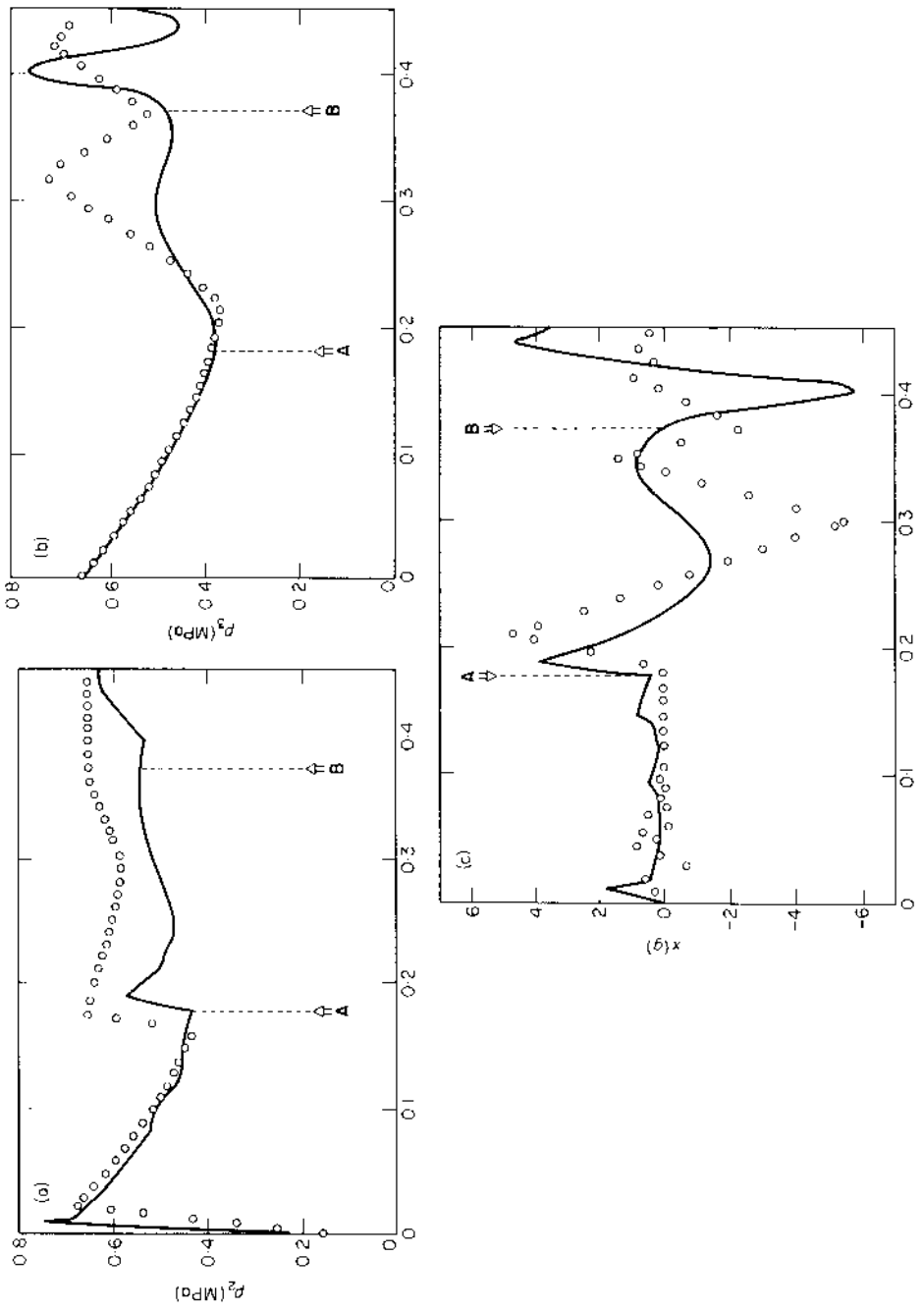

Figure 3. Comparison of measured and predicted time histories for example case II ($M_f = 11{\cdot}4$ kg, and $p_s = 0{\cdot}65$ MPa). ○, Measured; ——, predicted by using computer simulation. Symbols **A** and **B** indicate sleeve leaving the port at $x = h_u$, and stub entering the port at $x = S - h_d$, respectively, during the forward motion. (a) Driving pressure $p_2(t)$; (b) back pressure $p_3(t)$; (c) piston acceleration $\ddot{x}(t)$.

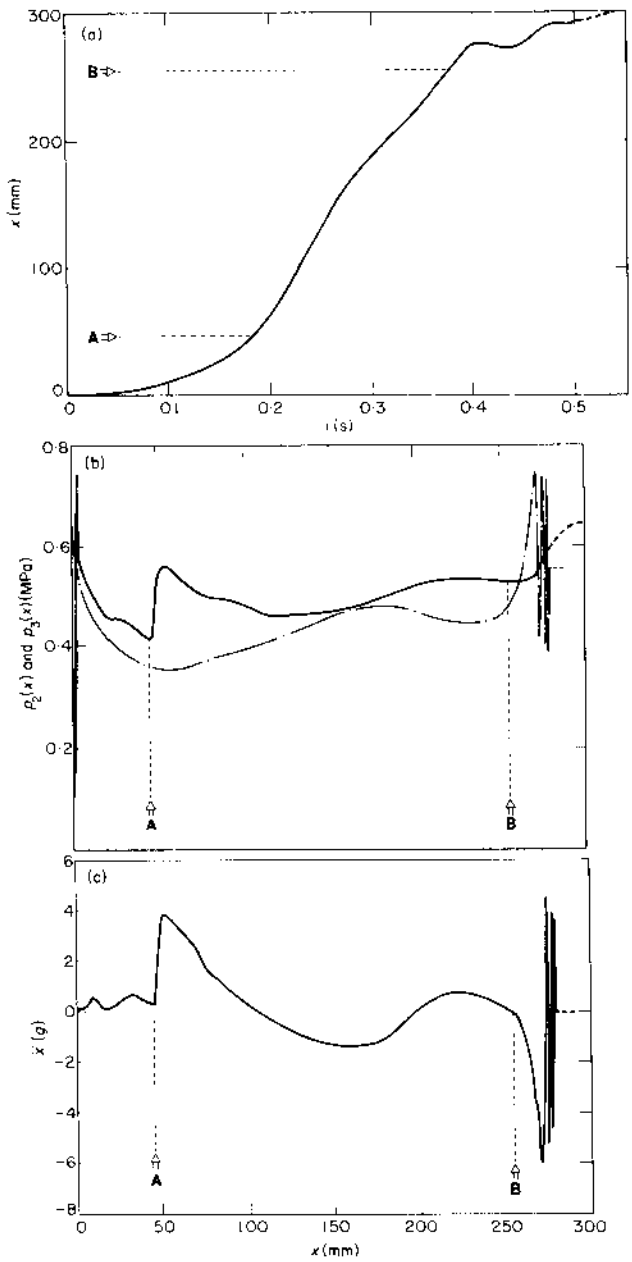

Figure 4. Predicted response curves for example case II ($M_t = 11{\cdot}4$ kg and $p_s = 0{\cdot}65$ MPa). Symbols **A** and **B** indicate sleeve leaving the port at $x = h_a$, and stub entering the port at $x = S = h_a$, respectively, during the forward motion. (a) Piston displacement time history $x(t)$; (b) pressure displacement curves: ——, driving pressure $p_2(x)$ and — · —, back pressure $p_3(x)$; (c) piston acceleration–displacement $\ddot{x}(x)$ curve.

Excellent correlations between simulation and experiment for $\ddot{x}^*$ and p_3^* are evident in Table 5. Measured and predicted cushion entrance velocity, i.e., the piston speed when the stub enters the port at $x = L$ are also compared in Table 5. The correlation between experiment and simulation is again very good, when it is considered that the measured velocities given in Table 5 are estimated by using $\ddot{x}(t)$ curves. To illustrate the agreement between theory and measurement further, some typical driving and back pressure, and acceleration time histories are presented in Figure 3. Here the events indicating pressure leaving the port (**A**) and the stub entering the port (**B**) are also shown; abrupt shifts in response variables are evident in these curves. Overall, the agreement between predicted and measured time histories is reasonable as both the trends and peak values are predicted. In fact, the comparisons for $p_2(t)$ and $p_3(t)$ are better than for $\ddot{x}(t)$. This suggests that the selected value of C is quite good; however, ζ_T selection could have been better.

In order to better indicate the piston dynamics and forcing function, some more simulated response curves, corresponding to the Figure 3 case, are given in Figure 4. Piston displacement time history is shown in Figure 4(c) for one stroke; the broken line at the end of the stroke indicates piston oscillations due to the mechanical impact. Such high frequency pneumatic and mechanical oscillations are also seen in Figures 3(b) and (c) for the back pressure $p_3(t)$ and piston acceleration $\ddot{x}(t)$. Abrupt shifts in the response curves at **A** and **B** should also be noted. For the untuned case, such sudden changes at **A** and **B** and oscillations due to the mechanical impact are very severe, as indicated by Table 4.

7. CONCLUDING REMARKS

Although the choice of damping ratio and discharge coefficients has been somewhat *arbitrary*, the computer simulation with such values still predicts cylinder performance reasonably well. To improve the present computer simulation model, a number of bench type experiments must be performed to develop better mathematical models for mechanical friction, fluid damping, leakage past the pistons, and discharge coefficients of numerous ports. A multi-degree of freedom model for piston motion should lead to more accurate predictions. Currently, efforts are underway to refine the computer simulation model along the lines described above. The overall system model will include mathematical descriptions for directional control valves, compressor or line source, and loading mechanisms.

The computer simulation model presented here has been extremely useful in not only understanding the basic shock-absorbing mechanism but also in evaluating different designs [17, 19]. The usage of this, or a similar, simulation model can be recommended to the fluid power control industry.

ACKNOWLEDGMENTS

We gratefully acknowledge Mr K. C. Mosier, II and Mr R. Herner of Mosier Industries, Inc., Brookville, Ohio for their generous support and encouragement.

REFERENCES

1. F. D. YEAPLE (editor) 1968 *Hydraulic and Pneumatic Power and Control.* New York: McGraw-Hill. See Chapter 10.
2. J. E. RUZICKA 1969 *Transactions of Society of Automotive Engineers* **77**, 2872–2886. Active vibration and shock isolation.

3. G. L. FOX and E. STEINER 1972 *Shock and Vibration Bulletin* **4**, 85–91. Transient response of passive pneumatic isolators.
4. C. M. HARRIS and C. E. CREDE (editors) 1976 *Shock and Vibration Handbook*. New York: McGraw-Hill. See Chapter 33.
5. M. S. HUNDAL 1978 *Journal of Mechanical Design* **100**, 236–241. Analysis of performance of pneumatic impact absorbers.
6. M. S. HUNDAL 1980 *Shock and Vibration Digest* **12**(9), 17–21. Pneumatic shock absorbers and isolators.
7. M. S. HUNDAL 1981 *Journal of Sound and Vibration* **76**, 273–281. Response of shock isolators with linear and quadratic damping.
8. M. S. HUNDAL 1982 *Shock and Vibration Bulletin* **52**(4), 161–168. Response of pneumatic isolator to standard pulse shapes.
9. M. S. HUNDAL 1982 *Journal of Sound and Vibration* **84**, 1–9. Passive pneumatic shock isolator: analysis and design.
10. G. O. ADAMS, R. D. BONNELL and J. E. FUNK 1968 *National Conference on Fluid Power*, 169–182. Computer simulation of fluid power systems.
11. Y. T. WANG, R. SINGH and D. A. GUENTHER 1982 *Journal of Sound and Vibration* **82**, 598–600. Modeling of an impulse-absorbing pneumatic cylinder.
12. A. H. SHAPIRO 1953 *The Dynamics and Thermodynamics of Compressible Fluid Flow*. New York: Ronald Press Company. See Chapter 4.
13. J. F. BLACKBURN, G. REETHOF and J. L. SHEARER (editors) 1960 *Fluid Power Control*. Cambridge, Massachusetts M.I.T. Press. See Chapter 16.
14. K. J. BELL and O. P. BERGELIN 1957 *Transactions of the American Society of Mechanical Engineers* **79**, 593–601. Flow through annular orifices.
15. S. FURUHAMA and T. TADA 1961 *Bulletin of Japan Society of Mechanical Engineers* **4**, 684–698. On the flow of gas through the piston-rings.
16. R. D. BLEVINS 1979 *Formulas for Natural Frequency and Mode Shape*. New York: Van Nostrand Reinhold. See Chapter 13.
17. H. C. YU 1982 *M.Sc. Thesis, The Ohio State University*. Experimental study of shock-absorbing air cylinders.
18. F. H. SPECKHART and W. L. GREEN 1976 *A Guide to Using CSMP*. Engelwood Cliffs, New Jersey: Prentice–Hall.
19. Y. T. WANG 1982 *M.Sc. Thesis, The Ohio State University*. Modeling of shock-absorbing air cylinders.

APPENDIX: LIST OF SYMBOLS

A	area
A	sleeve leaving the port
B	damping coefficient
B	stub entering the port
C	discharge coefficient
D	diameter
F	force
g_c	gravitational constant
h	thickness
K	spring stiffness
m, $\dot{m}$	fluid mass, mass flow rate
M	mechanical mass
p	pressure
R	gas constant
S	stroke, $(L - h_p)$
t	time
T	temperature
x, $\dot{x}$, $\ddot{x}$	piston displacement, velocity, acceleration
U	unit step function
V	volume
γ	specific heat ratio
ζ	damping ratio

Subscripts

1, 2, 3, 4	control volume indices
a	bleed orifice
b	cylinder port
d	downstream
e	exit
f	fluid (pneumatic)
i	inlet
j	control volume index
l	attached load
L	reservoir at the left end
m	mechanical
0	atmospheric
p	piston
q	piston stub
r	rod
R	reservoir at the right end
s	air supply
T	total
u	upstream
v	sleeve

Superscripts

$(\bar{})$	time-averaged
$(\ )^*$	peak value (absolute)